Visualizing brain ventricles volume changes during the cardiac cycle in MR images using motion magnification and optical flow algorithms.

Jessica Tawade
jt658@stanford.edu

Shai Limonchik
shailk@stanford.edu

Itamar Terem
iterem@stanford.edu

1. Abstract

The human brain undergoes constant motion and deformation due to a range of physiological dynamics. Blood vessels pulsation, together with cerebral spinal fluid (CSF) motion, apply changing pressure on brain tissue, which in turn, results in small motions and deformations [1, 2]. The physiological and biomechanical response of the human brain in vivo is thought to be altered in various neurological disorders [3, 4]. Thus, the ability to observe the manifestation of these disorders in the form of altered brain motion is thought to be of great interest. In this work, we propose the use of motion magnification and optical flow algorithms to observe subtle changes in brain ventricles in MR images. Our new processing methodology may open up exciting applications for neurological diseases that affect the biomechanics of the brain ventricles and brain fluids.

2. Introduction

Magnetic resonance imaging (MRI) is a powerful, non-invasive diagnostic medical imaging technique widely used to acquire detailed information about anatomy and function of different organs in the body, in both health and diseases [5]. Cardiac gated ('cine') MRI enables the acquisition of short video clips of brain tissue during the cardiac cycle [6]. Recently, amplified Magnetic Resonance Imaging (aMRI) has been introduced as a new brain motion detection and visualization method [7, 8], which enables one to dramatically amplify the brain tissue response due to blood pulsation and cerebrospinal fluid (CSF) motion. aMRI takes as an input a 'cine' MR data and uses phase based motion magnification algorithms [9] in order to reveal the sub voxel motion.

Optical flow algorithms enable the visualization and qualitative quantification of the apparent motion field [10], and can be applied to the amplified MRI data in order to characterize the brain ventricles motion. This could help understand the dynamics of what drives the passage of CSF through the ventricular system, and the extracellular fluid within the brain tissue, and open up exciting applications for a range of diseases and disorders that affect the biomechanics of the brain and brain fluids. These maps were visu-ally compared alongside PC-MR for their ability to capture the predominant brain tissue displacement which typically occurs in the cranial-caudal direction around the midbrain region.

3. Background/Related Work

Visualization of brain motion during the cardiac cycle with striking details was only recently achieved by amplified Magnetic Resonance Imaging (aMRI) [7, 8]. Before that, several methods have been introduced in order to visualize this pulsatile motion. Phase-contrast MRI, which uses a set of bipolar gradients to encode blood/brain velocity combined with cardiac synchronization, achieves high temporal resolution and enables the measurements of the brain tissue motion, blood and CSF flow [11]. A more recent quantitative tissue motion imaging technique, Displacement Encoded imaging with stimulated echoes (DENSE) MRI, encodes tissue displacement in the phase of the stimulated echo [12]. aMRI has advantages over both phase-contrast and DENSE-MRI since it has a shorter scan time. aMRI also has a higher temporal resolution than phase-contrast MRI, does not require phase-encoding in multiple directions to capture the full extent of brain motion, and is independent of the velocity encoding gradient aliasing effect.

4. Technical Approach

4.1. Data collection

Volumetric cardiac gated cine MRI datasets was shared by Matai institution in New Zealand (https://matai.org.nz). Scans were performed on volunteers using a 3T SIGNA Premier system (GE, USA), SuperG Gradients (80 mT/m @ 200 T/m/s), and a 46-channel head coil. The parameters for the 3D volumetric cine FIESTA sequence were as follows: FOV = 23cm2, matrix size = 256 x 256, TR/TE/flip-angle = 2.9ms/1ms/25°, Hyperkat 8 acceleration, partition-thickness of 1.2mm (resolution of 1.2 x 1.2 x 1.2mm), peripheral pulse gating. 116 slices were used for whole brain coverage and retrospectively binning to 20 cardiac phases was applied. The 3D volumetric cine FIESTA sequence

took approximately 2.5 minutes. In total. 5 volumetric data sets were shared.

In order to compare qualitatively the optical flow maps to a ground truth another data set of cine PC-MRI data and 3D volumetric aMRI data on a same volunteer using the 3T GE Signa system, with the following parameters: FOV = 23cm2, velocity encoding = 1cm/s, matrix size = 256 x 256, TR/TE/flip-angle = 50ms/12ms/10°. Phase-encoding was performed in the R-L direction in the axial plane, and in the S-I direction for the sagittal and coronal planes. The resulting images were masked to remove the background noise and highlight the brain motion in these directions of interest.

4.2. Motion magnification

aMRI is based on the Eulerian perspective for the flow field, where the properties of a voxel of fluid, such as pressure and velocity, evolve over time. This differs from the Lagrangian perspective, where the trajectory of particles is tracked over time. In the Eulerian approach to motion magnification, the motion is not explicitly estimated, but rather magnified by amplifying temporal intensity changes at fixed voxel [8], assuming that the motion is subtle (sub-voxel).

aMRI starts by decomposing the data into scales and orientations using the 3D steerable pyramid. Initially the image is separated into low and high-pass subbands. The low-pass image is then divided into 6 oriented bandpass subbands and a lower-pass subband. This last one is then subsampled by a factor of 2, both in the x, y and z directions. The recursivity is achieved by inserting another level of decomposition in the lower branch.

The scales (levels) basis functions are band pass filters in the frequency domain. They are calculated in polar coordinates by multiplying a low pass filter L_{s-1} of the previous scale with a high pass filter H_s of the current scale. The low pass and high pass filters for each scale are given by the following equations:

$$
H_s(r) \begin{cases} 1, & \frac{r}{s} \geq 1 \\ \left| cos\left(\frac{\pi}{2} log_2\left(\frac{r}{s}\right)\right)\right|, & 0.5 < \frac{r}{s} < 1 \\ 0, & 0 < \frac{r}{s} \leq 0.5 \end{cases} \quad (1)
$$

$$
L_s(r) = \begin{cases} 0, & \frac{r}{s} \geq 1 \\ \left| sin\left(\frac{\pi}{2} log_2\left(\frac{r}{s}\right)\right)\right|, & 0.5 < \frac{r}{s} < 1 \\ 1, & 0 < \frac{r}{s} \leq 0.5 \end{cases} \quad (2)
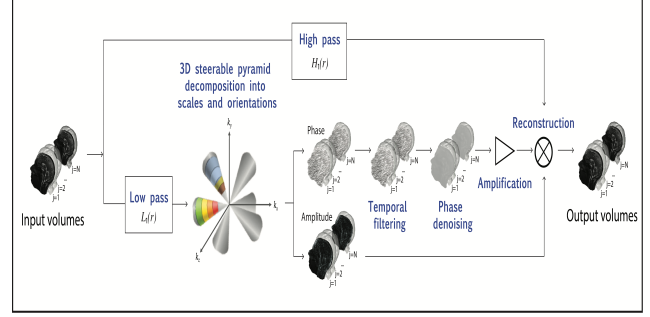$$

Figure 1. The amplified MRI (aMRI) algorithm pipeline. The volumetric/multi-slice cine MRI is decomposed by the 3D complex steerable pyramid into scales and orientations. The colors represent the frequency response of the different filters (scales and orientations). Each filter is a bandpass with specific orientation and satisfies equation 5. The phases of the decomposition are separated from the amplitude component, and independently temporally band pass filtered at each spatial location, orientation, and scale. The filtered phases are then "spatially" filtered again to increase the phases SNR using amplitude-weighted Gaussian spatial smoothing, and then multiplied by an amplification parameter and added to the original amplitude component. The 4D data is then reconstructed to produce an amplified 4D movie.

Where s is the scaling factor of the level, and the band pass filter for the level is given by,

$$
B_s(r) = H_s(r) \times L_{s-1}(r) \quad (3)
$$

The angular filters are the 3D cones oriented along the six vertices of cuboctahedron (Table 1) and satisfy the following equation in the frequency domain:

$$
B_j(k_x, k_y, k_z) = \frac{(\alpha_j k_x + \beta_j k_y + \gamma_j k_z)^2}{k_x^2 + k_y^2 + k_z^2}, \quad (4)
$$

$j = 0, 2, ..., 5$

Where α_j, β_j and γ_j are the direction of the axes of symmetry of the six basis filters B_j. The resulting filter in the frequency domain (Figure 1) for each level and orientation is given by:

$$
A_{s,j}(k_x, k_y, k_z) = B_s(r) \times B_j(k_x, k_y, k_z) \quad (5)
$$

Where, $r = \sqrt{k_x^2 + k_y^2 + k_z^2}$

And every scale and orientation in the decomposition is constructed as follow:

$$
I_{s,j}(x, y, z) = F^{-1}\left\{ F\left\{ I(x, y, z)\right\} \times A_{s,j}\right\} \quad (6)
$$

Where s and j are the scaling factor and orientation direction respectively, $F\left\{I(x, y, z)\right\}$ is the Fourier transform

of the image, and F^{-1} is the inverse Fourier transform. The steerable pyramid decomposition outputs a complex number (amplitude and phase) at each scale and orientation. The phases are temporarily band-passed in order to isolate the cardiac temporal frequency and to remove any DC component. In addition, in order to enable motion magnification with minimal noise artifacts, the band-passed phases are spatially filtered with an amplitude-weighted Gaussian smoothing filter. Next, the band-passed phases are multiplied by a user-defined amplification factor, α, and added to the original phase component. Attenuation of motion of the other temporal frequencies is achieved by adding the band-passed phases to a reference phase image/volume, which in our case was chosen to be the first volume. The volume is then reconstructed to synthesize an amplified 4D movie with the desirable range of temporal frequencies.

The following parameters were used: amplification factor $\alpha = 25$, band-pass filter of the heart rate frequency (± 0.1) in addition to attenuating the motion related to all other temporal frequencies, and amplitude-weighted Gaussian smoothing with $\sigma = 5$. The amplification factor α was chosen according to the original 2D aMRI [8] study as $\delta(t)\alpha < \frac{\lambda}{2}$, where $\delta(t)$ is a displacement function, and λ is the spatial wavelength. By assuming a maximum displacement of the brain stem (midbrain, pons, and medulla) of approximately $\delta(t) = 187\ \mu m$ [13], and minimum resolve wavelength $\lambda = 4 \times 2.4mm$ (amplitude-weighted Gaussian smoothing), we chose an α within the boundary $\alpha < 25.6$, that supports sufficient amplification and with minimum artifacts and distortions.

4.3. Optical Flow

Once the amplification process is complete, the next step is to generate optical flow maps by applying the Farneback optical flow algorithm to our aMRI data. These optical flow maps will not only provide a clear visualization of the amplified motion, but will also capture the predominantly midbrain tissue displacement. The Farneback algorithm evaluates changes within a relatively small, neighborhood of each data vector using the following steps [10]:

1. Model the aMRI image with polynomial basis functions which are weighted by an applicability function that determines the neighborhood's importance

2. Use the modeled signal to find the optimal position and orientation needed to align a floating image f_2 to a reference image f_1

3. Using the orientation tensors, compute displacement between the two images

Step 1 involves using signal decomposition techniques to locally decompose the aMRI images. Using normalized
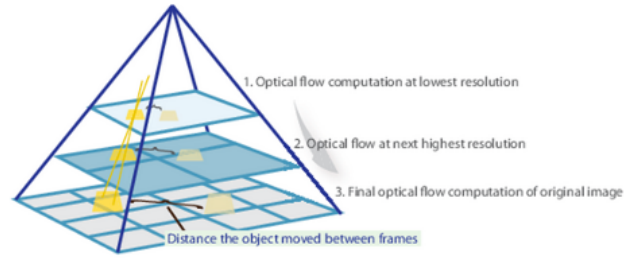

Figure 2. Multiscale Iterative Pyramid for Optical Flow [10, 14]

convolution and polynomial basis functions, the images can be approximated using the following polynomial:

$$f(\mathbf{x}) \sim \mathbf{x}^T \mathbf{A} \mathbf{x} + \mathbf{b}^T \mathbf{x} + c \qquad (7)$$

where $\mathbf{A}$ is a symmetric matrix, $\mathbf{b}$ is a vector, and c is a scalar [10]. Estimates for the polynomial coefficients can be found by fitting the polynomial for each image using weighted least squares within a neighborhood [10].

After solving for the polynomial basis functions, steps 2 and 3 involve exploring the relationship between the floating image f_2 the reference image f_1. The relationship between the two images can be modeled using the following equation:

$$f_2(\mathbf{x}) = f_1(\mathbf{x} - \mathbf{d}) \qquad (8)$$

where $\mathbf{d}$ represents the displacement vector between the two images [10]. Equation 7 can be used to further expand Equation 8 and help solve for the displacement between the two images over the neighborhood region. The mathematical details can be found in [10], but ultimately the displacement vector is determined to be:

$$\mathbf{d} = -\frac{1}{2}\mathbf{A}_1^{-1}(\mathbf{b}_2 - \mathbf{b}_1)$$

This registration process can be repeated across a multiscale iterative pyramid from lowest to highest resolution in order to achieve a large range of transformation [10].

As seen in Figure 2 [10, 14], the resolution increases as we move to lower levels of the pyramid and at each level of the pyramid, the Farneback algorithm is performed using the corresponding resolution of the level in order to calculate the displacement vector. The displacement tracking starts at the lowest resolution level and the result of each preceding level is used to form an initial guess for point locations in the next level [10]. This process continues to track the displacement at higher resolution levels until the original image resolution is reached, ultimately leading to a fully developed optical flow map [10]. Algorithm parameters such as the neighborhood size, filter size, and number of pyramid levels can be altered to help enable the algorithm to [10, 14]:

- Handle larger pixel motions

- Yield more robust estimation of optical flow

- Become more robust to image noise

- Handle fast motion detection

As mentioned in Section 2, the evaluation of the motion will be conducted qualitatively, by using PC MRI (which provides information about the velocity field) in order to produce vector directions. The velocity changes seen in PC MRI can be used to generate videos which will be treated as ground truth and compared against the optical flow maps produced by the Farneback algorithm.

5. Experiments

A dataset of 5 volumetric gated cine magnetic resonance images (MRI) of the brain was shared by the Matai institution in New Zealand. Each of the 5 data sets was processed by the Amplified MRI algorithm. After, The optical flow algorithm (Farneback algorithm) was applied on the amplified data, and the evaluation of the motion was conducted qualitatively, by using Phase Contrast (PC) MRI, a well known velocity encoding acquisition. The velocity changes seen in PC MRI can be used to generate videos which was treated as ground truth and compared against the optical flow maps produced by the Farneback algorithm.

5.1. Amplification experiments

The first part was to test the implementation of the algorithm. Figures 3, together with the video link: `https://web.stanford.edu/~iterem/axial.mov` , show that the aMRI algorithm was implemented correctly. Amplification of sub voxel motion due to heart pulsation is clearly seen in all three planes (sagittal, coronal and axial), where without amplification (original data) no motion is seen. In order to visualize the amplification in the form of an image, we calculate the difference maps (figure 3) from two frames which exhibited the maximum displacement (frame 1 and frame 10).

The second step was to optimized the parameters of magnification algorithm. As was stated in the motion magnification section (4.2) there are 3 main parameters that affects the results: Temporal frequencies band, amplification factor, and smoothing parameters. In this work we focused on the heart rate frequency, so we band-pass filter the heart rate frequency (± 0.1) in addition to attenuating the motion related to all other temporal frequencies. The amplification factor was chosen according to the mathematical analysis that was introduce in the motion magnification section (4.2). In addition, in order to verify that the mathematical derivation yield good approximation, we tested different amplification factors $\alpha = [15\,25\,30\,40]$ together with different smoothing factors $\sigma = [2.5, 5, 7.5, 10]$ and inspected the magnify motion

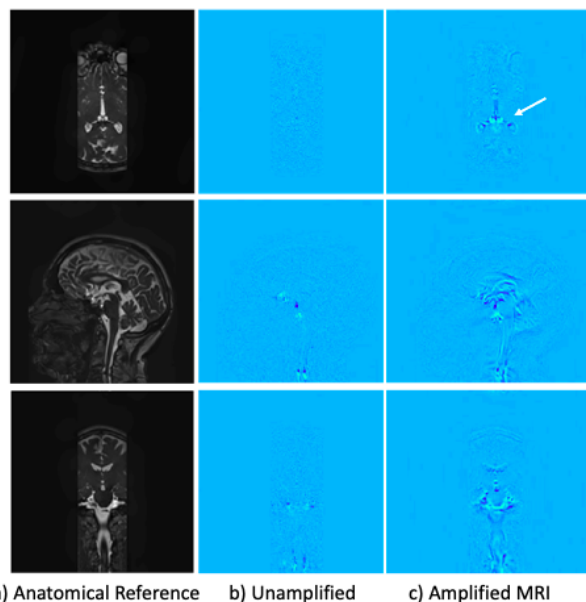a) Anatomical Reference   b) Unamplified   c) Amplified MRI

Figure 3. aMRI output. (a) anatomical reference, and difference maps for (b) unamplified, (c) aMRI. Difference maps were calculated from two frames which exhibited the maximum displacement (frame 1 and frame 10). aMRI captures the complete motion, particularly in the axial plane where the 'piston-like' motion. (white arrow).

by looking for motion artifacts and noise. The two parameters were tuned together because the amount of smoothing is directly related to the amount of possible amplification. Where larger smoothing enable larger magnification, but with lower resolution (large smoothing result in loosing motion of higher spatial wavelength). Figure 4 depict an example of this analysis, where we see motion artifacts that are caused by larger magnification factor ($\alpha 40$), when choosing smoothing factor of $\sigma 5$. We noticed that while small amplification factor does not result in motion artifact, the motion was difficult to perceive. On the other hand, larger amplification factor resulted in significant motions artifacts (figure 4). We found that the combination of amplification factor of $\alpha = 25$ and amplitude-weighted Gaussian smoothing with $\sigma = 5$ yield enough motion, with minor motion artifacts as was suggested by the mathematical derivation.

5.2. Optical Flow experiments

In order to generate optical flow maps that accurately represent the motion of the brain ventricles, we ran experiments with different parameters of the Farneback optical flow algorithm on the aMRI images. The first experiment that we ran involved altering the Gaussian filter size while keeping all other parameters of the algorithm fixed. The Gaussian filter is a $n \times n$ filter that is used to average over neighborhoods after the displacement is computed
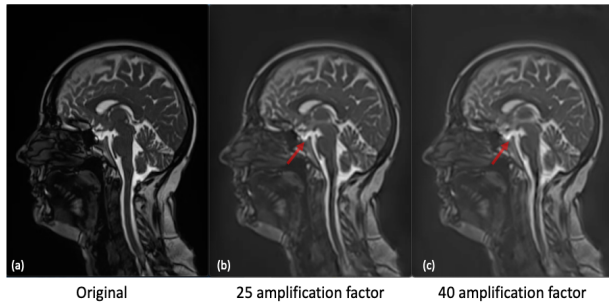
Figure 4. Comparison between two different amplification factors. (a) the original MRI video, (b) the same video amplified with amplification factor of 25 and (c) with 40. As can be seen (red arrows) motion artifacts exist in the movie with 40 amplification factor compared to 20

[14]. Due to the structure of the Gaussian filter, pixels near the border are weighted less because the Farneback algorithm assumes that the coefficients of the polynomial estimated during the polynomial expansion transform are less accurate near the border [14]. Ultimately, the goal of the filter is to reduce image noise and theoretically, increasing the filter size allows the Farneback algorithm to better handle image noise and fast motion detection [14].

We experimented with 3 different Gaussian filter sizes: 3×3, 9×9, and 15×15 (dimensions are in pixels). From the first row of Figure 7 (Figures 7a, 7b, 7c), we can see that with the smallest filter size (3×3), majority of the displacement vectors are centered over the ventricle region in Figure 7a. This is a good sign because it means that the algorithm was able to recognize that majority of the motion occurs in the ventricle region. However, the magnitude of most of the displacement vectors is quite small and there is also a large displacement vector in the bottom right of the ventricle region which incorrectly indicates that there is a overwhelmingly large motion in the bottom right part of the brain ventricle compared to other parts of the ventricle. Due to these inconsistencies, we decided to increase the filter size to 9×9 and 15×15. With the 9×9 Gaussian filter, we are able to gather more information about the ventricle motion and overall brain motion because more displacement vectors appear in the ventricle region and the surrounding regions (See Figure 7b). The inconsistencies in vector magnitude that appeared with a smaller filter size are also not apparent when using a 9×9 filter size. Our best results came from using the 15×15 Gaussian filter size. From Figure 7c, we can see that the 15×15 Gaussian filter not only shows the motion within the ventricles, but also shows the motion of the brain region adjacent to the brain ventricles. This figure provides more context about the overall brain motion
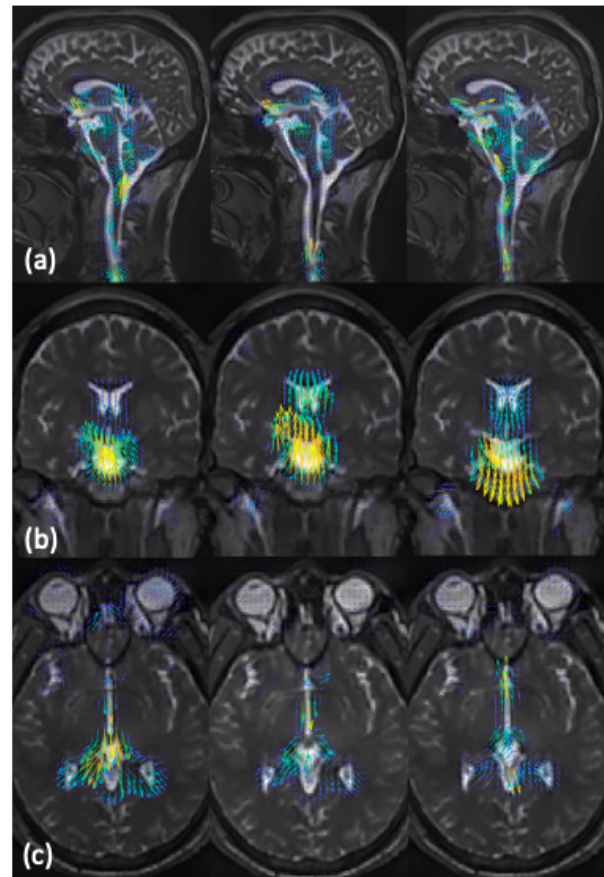

Figure 5. Optical flow maps calculated from aMRI for (a) sagittal, (b) coronal, and (c) axial planes. Here we show successive phases of motion at approximately third intervals of cardiac cycle. The optical flow maps capture the brain tissue motion over time and display the physical change in shape of the ventricles by the relative movement of the surrounding tissues.

compared to smaller filter sizes. As a result, we decided to use a 15×15 Gaussian filter for our final results in Figure 5.

In addition to filter size, we also experimented with pixel neighborhood size. Theoretically, increasing the neighborhood size helps to blur the motion in the Farneback algorithm, yielding a more robust optical flow estimation [14]. We experimented with 3 different neighborhood sizes: 3×3, 9×9, and 15×15 (dimensions are in pixels). From Figures 7d and 7e, we can see that using smaller neighborhood sizes (3×3 and 9×9) only seems to capture small amounts of local motion within the neighborhood and fails to recognize the large amount of motion stemming from the brain ventricles. Furthermore, Figures 7d and 7e also generate displacement vectors outside of the brain slice. Increasing the neighborhood size to 15×15 allowed for the Farneback algorithm to generate polynomials for
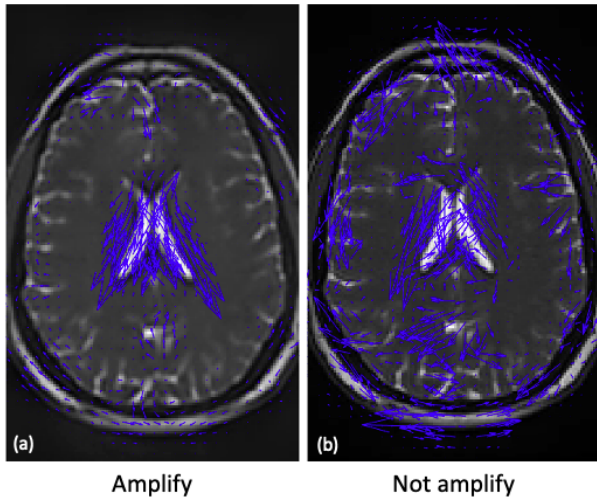
Figure 6. Optical flow maps calculated from the amplify (a) and original(b) videos. As we can see the optical flow maps of he original video contain significant errors and does not resemble the real motion.
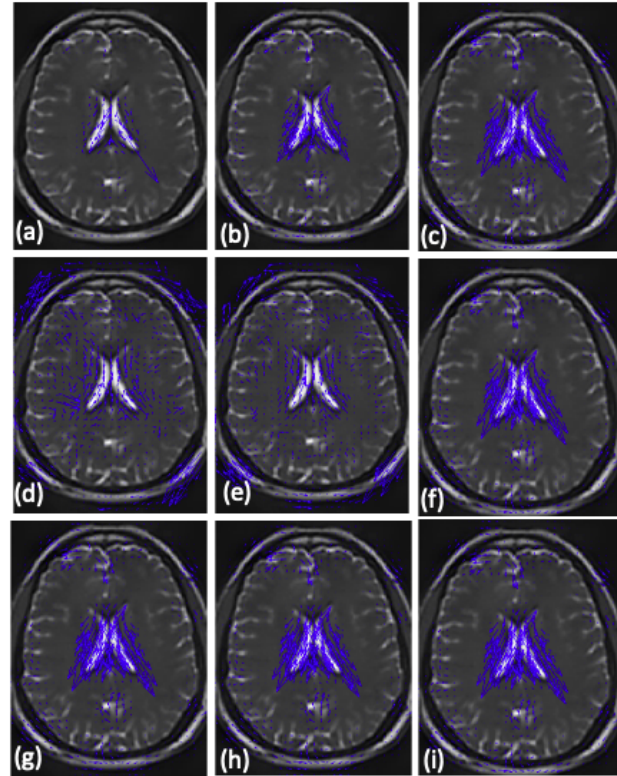

Figure 7. Optical flow maps with different parameters calculated from aMRI. First row (a,b,c) with different Gaussian filter sizes [3,9,15] respectively. Second row (d,e,f) with different neighborhood sizes [3,9,15] respectively. Third row (g,h,i) with different pyramids levels [3,5,7] respectively. As we can see the pyramid size was not affecting the result significantly compare to the Gaussian and the neighborhood sizes.

each neighborhood that better captured the overall brain ventricle motion and ignored the smaller, local motions in the surrounding regions. As a result, we decided to use a 15×15 neighborhood size for our final results in Figure 5.

The last parameter we explored was the number of pyramid levels that the algorithm utilizes. Each pyramid level runs the Farneback algorithm using a different image resolution. This process helps to better represent large displacements between image frames [10]. We tried using 3, 5, and 7 pyramid levels. Interestingly, increasing the number of levels had little to no effect on the optical flow maps (Figures 7g-7i). A reason for this result could be that the displacement between frames of the aMRI images were not large enough to need more pyramid levels. As a result, we arbitrarily decided to use 7 pyramid levels for our final results in Figure 5.

Once we were able to set our optical flow algorithm parameters, we were able to use the aMRI images to generate optical flow maps for different image planes and at various intervals of the cardiac cycle. Figure 5 together with the video link: `https://web.stanford.edu/~iterem/Supporting_Video_S8.mp4` shows the optical flow maps for the sagittal (Figure 5a), coronal (Figure 5b), and axial planes (Figure 5c) each of which are displayed at three different points in time. We chose to color code these optical flow maps in order to better demonstrate the difference in magnitude between the displacement vectors. The optical flow maps for each of these planes not only allow us to observe the brain tissue

motion over time, but also allow us to visualize the physical change in shape of the ventricles by the relative movement of the surrounding tissue. The maps also reveal information about parts outside of the brain. For example, in Figure 5c, we are able to visualize slight movement in the eyes. These results open up exciting opportunities for scientists to further explore the mechanisms of brain motion.

The use of optical flow maps also helped us to visualize the importance of aMRI. Figure 6b demonstrates the difficulty of being able to extract information about brain motion from the un-amplified MRI. The displacement vectors are randomly dispersed and don't seem to show any unified motion throughout the brain. The amplification process in aMRI provides the optical flow algorithm with more information that can be used to generate a better representation of the motion in the ventricles and surrounding regions as seen in Figure 6a.

5.3. Comparison to Phase contrast

Quantitative evaluations of the amplified optical flow maps was not possible in this work. This is mainly because aMRI is a new methodology that is still under investigation to see if quantitative displacement measurements can be extracted from the amplified output. In order to qualitative evaluate our result, we compared them to phase contrast MRI. Phase contrast MRI is an MR acquisition which enables direct measurements of the velocity filed. In both optical flow aMRI and cine PC-MRI, the general characteristic of brain motion was found to be similar (Figure 8 and `https://web.stanford.edu/~iterem/PC.mp4`). On aMRI, this motion was clearly captured in the form of vectors by the optical flow map, which visually represented the velocity fields seen on PC-MR.
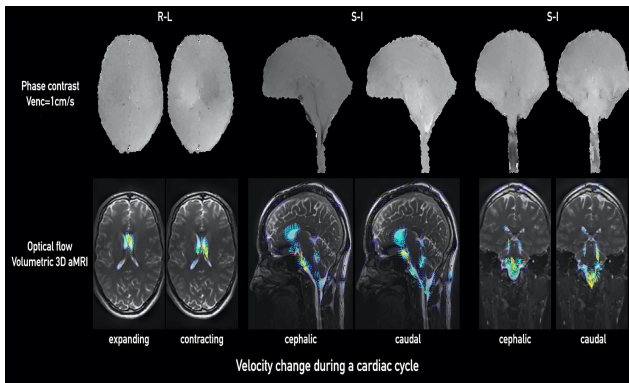

Figure 8. Comparison between Phase Contrast (PC)-MRI (top) and optical flow maps calculated from aMRI (bottom) for (a) sagittal, (b) coronal, and (c) axial planes. Here we show the pair of 12th and 19th phases of a cardiac cycle (the same total number of 20 phases collected for each of the PC-MRI and volumetric 3D aMRI methods). The optical flow maps capture the relative brain tissue deformation over time and the physical change in shape of the ventricles by the relative movement of the surrounding tissues.

6. Conclusion

In this project we used motion magnification and optical flow algorithms in order to reveal and asses the sub voxel motion of the brain ventricles due to blood pulsation and CSF motion. The results showed that the aMRI algorithm was implemented correctly and enable the visualization of amplified cardiac- and CSF-induced brain tissue and ventricles motion. The optical flow maps of aMRI captured the motion in the form of vectors, and show similar motion characteristic as seen in PC-MR. The new processing methodology may open up exciting applications for neurological diseases that affect the biomechanics of the brain ventricles and brain fluids.

References

[1] Mestre H et al. Flow of cerebrospinal fluid is driven by arterial pulsations and is reduced in hypertension. *Nat Commun*, 9(9):4878, 2018.

[2] Hirsch S et al. In vivo measurement of volumetric strain in the human brain induced by arterial pulsation and harmonic waves. *Magn. Reson. Med*, 70(9):671–683, 2013.

[3] Bradley WG Jr. Magnetic resonance imaging of normal pressure hydrocephalus. *Semin Ultrasound CT MR*, 37(2):120–128, 2016.

[4] Tsao et al. Relations of arterial stiffness and endothelial function to brain aging in the community. *Neurology*, 81(2):984–991, 2013.

[5] Vijayalaxmi, Mahsa Fatahi, and Oliver Speck. Magnetic resonance imaging (MRI): A review of genetic damage investigations. *Mutat. Res. - Rev. Mut. Res.*, 764(6):51–63, 2015.

[6] Oliver Bieri and Klaus Scheffler. Fundamentals of balanced steady state free precession MRI. *J. Magn. Reson. Imaging*, 38(1):2–11, 2013.

[7] Samantha J Holdsworth, Mahdi Salmani Rahimi, Wendy W Ni, Greg Zaharchuk, and Michael E Moseley. Amplified magnetic resonance imaging (aMRI). *Magn. Reson. Med.*, 75(6):2245–2254, 2016.

[8] Itamar Terem, Wendy W Ni, Maged Goubran, Mahdi Salmani Rahimi, Greg Zaharchuk, Kristen W Yeom, Michael E Moseley, Mehmet Kurt, and Samantha J Holdsworth. Revealing sub-voxel motions of brain tissue using phase-based amplified MRI (aMRI. *Magn. Reson. Med.*, 80(6):2549–2259, 2018.

[9] Neal Wadhwa, Michael Rubinstein, Frédo Durand, and William T Freeman. Phase-based video motion processing, 2013.

[10] Gunnar Farnebäck. Two-frame motion estimation based on polynomial expansion. In *Scandinavian conference on Image analysis*, pages 363–370. Springer, 2003.

[11] Pelc N Enzmann DR. Brain motion measurement with phase-contrast mr imaging. *Radiology*, 185(9):653–660, 1992.

[12] Xiaodong Zhong et at. Balanced multipoint displacement encoding for dense mri. *Magn Reson Med*, 61(4):981–988, 2009.

[13] Oshinski J. Zhong X. Loth F. Pahlavian, S. H. and R Amini. Regional quantification of brain tissue strain using displacement-encoding with stimulated echoes magnetic resonance imaging. *ASME. J Biomech Eng.*, 140(8):2549–2259, 2018.

[14] Object for estimating optical flow using farneback method - matlab. Available at `https://www.mathworks.com/help/vision/ref/opticalflowfarneback.html`.

7. Supplementary Materials

Please see the following link to view all code resources used in the development of our project: `https://github.com/ItamarTerem/CS231-Project`